HHS Public Access

Author manuscript

Nat Genet. Author manuscript; available in PMC 2020 April 15.

Published in final edited form as:

Nat Genet. 2019 September ; 51(9): 1308–1314. doi:10.1038/s41588-019-0475-y.

Mutations in *RABL3* alter KRAS prenylation and are associated with hereditary pancreatic cancer

Sahar Nissim[1,2,3,4], **Ignaty Leshchiner**[2,5], **Joseph D. Mancias**[3,6], **Matthew B. Greenblatt**[7], **Ophélia Maertens**[2], **Christopher A. Cassa**[2], **Jill A. Rosenfeld**[8], **Andrew G. Cox**[9,10], **John Hedgepeth**[2], **Julia I. Wucherpfennig**[2], **Andrew J. Kim**[2], **Jake E. Henderson**[2], **Patrick Gonyo**[11], **Anthony Brandt**[11], **Ellen Lorimer**[11], **Bethany Unger**[11], **Jeremy W. Prokop**[12], **Jerry R. Heidel**[13], **Xiao-Xu Wang**[3], **Chinedu I. Ukaegbu**[3], **Benjamin C. Jennings**[14], **Joao A. Paulo**[6], **Sebastian Gableske**[3], **Carol A. Fierke**[14], **Gad Getz**[5,15], **Shamil R. Sunyaev**[2,16], **J. Wade Harper**[6], **Karen Cichowski**[2,3], **Alec C. Kimmelman**[17], **Yariv Houvras**[18], **Sapna Syngal**[1,3], **Carol Williams**[11], **Wolfram Goessling**[2,3,4,5,19,20,*]

[1]Gastroenterology Division, Brigham and Women's Hospital, Harvard Medical School, Boston, MA, USA.

[2]Genetics Division, Brigham and Women's Hospital, Harvard Medical School, Boston, MA, USA.

[3]Dana-Farber Cancer Institute, Boston, MA, USA.

[4]Harvard-MIT Division of Health Sciences and Technology, Cambridge, MA, USA.

[5]The Eli and Edythe L. Broad Institute of MIT and Harvard, Cambridge, MA, USA.

[6]Department of Cell Biology, Harvard Medical School, Boston, MA, USA.

[*]**Correspondence and requests for materials** should be addressed to W.G. wgoessling@partners.org.

Author contributions

S.N. and W.G. conceived and designed the overall project. S.S. and C.I.U. assisted with selecting the family, gathering the clinical histories and collecting DNA samples under human subject IRB-approved protocols. S.N., W.G. and I.L. designed the WGS analysis. I.L. performed the WGS analysis and candidate variant filtering. S.N., J.W., A.J.K., J.E.H., A.G.C. and J.H. designed and generated the zebrafish *rabl3* mutant lines and performed the cancer studies. J.R.H. and S.N. performed zebrafish histology preparation and analysis. J.D.M. performed and analyzed the AP–MS experiments and CompPASS suite protein interactomics. S.N., W.G. and C.W. conceived and designed the in vitro immunoprecipitation, prenylation assays and HEK293T cell proliferation assays, and P.G., A.B., E.L. and B.U. performed these experiments. S.N. and O.M. designed and performed RASless MEF experiments. J.W.P. performed protein structural modeling. B.C.J. and C.A.F. designed and performed purification of recombinant protein. J.A.P., S.G. and J.D.M. assisted with mass spectrometry analysis. Y.H. assisted with RNA-seq data analysis. M.B.G. performed the zebrafish μCT and bone histomorphometric analysis. O.M., X.W. and J.D.M. provided assistance with tissue culture experiments. C.A.C. and J.A.R. provided analysis of clinical exome sequencing data. C.A.C. and I.L. provided analysis of variants in the Exome Aggregation Consortium. J.W.H., G.G., S.R.S., K.C. and A.C.K. provided overall input. S.N. and W.G. wrote the manuscript. All authors reviewed and edited the manuscript.

Additional information

Supplementary information is available for this paper at https://doi.org/10.1038/s41588-019-0475-y.

Reprints and permissions information is available at www.nature.com/reprints.

Publisher's note: Springer Nature remains neutral with regard to jurisdictional claims in published maps and institutional affiliations.

Data availability

RNA-seq data are available through GEO under accession GSE129081. Interacting proteomic data are available through Peptide Atlas under accession PASS01355. Additional data generated in this study are available within the paper and in the supplementary information.

Online content

Any methods, additional references, Nature Research reporting summaries, source data, statements of code and data availability and associated accession codes are available at https://doi.org/10.1038/s41588-019-0475-y.

[7]Department of Pathology and Laboratory Medicine and the Hospital for Special Surgery, Weill Cornell Medical College, Cornell University, New York, NY, USA.

[8]The Department of Molecular and Human Genetics, Baylor College of Medicine, Houston, TX, USA.

[9]Peter MacCallum Cancer Centre, Melbourne, Victoria, Australia.

[10]Department of Biochemistry and Molecular Biology, University of Melbourne, Parkville, Victoria, Australia.

[11]Cancer Center and Department of Pharmacology and Toxicology, Medical College of Wisconsin, Milwaukee, WI, USA.

[12]HudsonAlpha Institute for Biotechnology, Huntsville, AL, USA.

[13]Carlson College of Veterinary Medicine, Oregon State University, Corvallis, OR, USA.

[14]Department of Chemistry, University of Michigan, Ann Arbor, MI, USA.

[15]Cancer Center and Department of Pathology, Massachusetts General Hospital, Harvard Medical School, Boston, MA, USA.

[16]Department of Biomedical Informatics, Harvard Medical School, Boston, MA, USA.

[17]Department of Radiation Oncology, Perlmutter Cancer Center, New York University School of Medicine, New York, NY, USA.

[18]Weill Cornell Medical College and New York Presbyterian Hospital, New York, NY, USA.

[19]Harvard Stem Cell Institute, Cambridge, MA, USA.

[20]Division of Gastroenterology, Massachusetts General Hospital, Harvard Medical School, Boston, MA, USA.

Abstract

Pancreatic ductal adenocarcinoma is an aggressive cancer with limited treatment options[1]. Approximately 10% of cases exhibit familial predisposition, but causative genes are not known in most families[2]. We perform whole-genome sequence analysis in a family with multiple cases of pancreatic ductal adenocarcinoma and identify a germline truncating mutation in the member of the RAS oncogene family-like [3] (*RABL3*) gene. Heterozygous *rabl3* mutant zebrafish show increased susceptibility to cancer formation. Transcriptomic and mass spectrometry approaches implicate RABL3 in RAS pathway regulation and identify an interaction with RAP1GDS1 (SmgGDS), a chaperone regulating prenylation of RAS GTPases[3]. Indeed, the truncated mutant RABL3 protein accelerates KRAS prenylation and requires RAS proteins to promote cell proliferation. Finally, evidence in patient cohorts with developmental disorders implicates germline *RABL3* mutations in RASopathy syndromes. Our studies identify *RABL3* mutations as a target for genetic testing in cancer families and uncover a mechanism for dysregulated RAS activity in development and cancer.

To identify additional genes involved in hereditary pancreatic ductal adenocarcinoma (PDAC), we performed whole-genome sequencing (WGS) and analysis on a family with a

striking history of five relatives with PDAC, and multiple other occurrences of cancer spanning multiple generations, consistent with a highly penetrant autosomal dominant mode of inheritance (Fig. 1a). Germline mutations in known cancer risk genes[2], including *BRCA2* and *p16/CDKN2A*, had previously been excluded. Candidate variants were identified by WGS of the proband (PDAC, age 48) and her paternal uncle (PDAC, age 80) and analysis with our computational algorithm[4] which is based on the hypothesis that causative variants are highly penetrant and autosomal dominant, rare, heterozygous in both affected individuals and result in protein-altering variation (Fig. 1b). We identified a variant (hg19 chr3: g.120449574 G>T, rs200612497) in *RABL3* that causes a premature nonsense mutation at amino acid 36 (*RABL3_p.Ser36**) (Fig. 1c). WGS confirmed the absence of protein-altering variants in known PDAC risk genes. Sanger sequencing of other available family members revealed significant co-segregation of the mutant *RABL3* allele with cancer (Fig. 1a, $P = 0.0476$). The Exome Aggregation Consortium (ExAC) database contains only one occurrence of this variant, confirming the identified mutation as a very rare event.

To functionally validate the causality of this allele in cancer, mutant RABL3_p.Ser36* was expressed in HEK293T cells, resulting in enhanced cell proliferation consistent with an oncogenic effect (Fig. 2a). To assess cancer promotion in vivo, we recapitulated the mutation in zebrafish. The zebrafish ortholog, Rabl3, is highly conserved with 100% identity through the first 50 amino acids, including position 36 where the human familial nonsense mutation occurs (Fig. 2b). The *rabl3* mutant zebrafish were generated by CRISPR–Cas9 genome editing, resulting in mutant alleles that encode a premature protein truncation (labeled Rabl3-TR, Supplementary Fig. 1a). The impact of these alleles on cancer was interrogated in two well-established independent tumor models, utilizing either genetic predisposition or chemical carcinogenesis. Both approaches reveal that zebrafish heterozygous for Rabl3-TR develop cancers at a statistically significant accelerated rate and with greater frequency than their Rabl3 wild-type siblings. (1) The *tp53*-null mutant zebrafish are predisposed to developing malignant peripheral nerve sheath tumors (MPNSTs)[5]. Heterozygosity for the mutant *rabl3-TR*^{52} allele in a *tp53*-null background accelerates formation of MPNSTs by over 3 months (Fig. 2c; $N = 64$, $P = 0.0011$), while histology and anatomical distribution of periocular (54.5%) and abdominal (45.5%) MPNSTs in heterozygous *rabl3-TR*^{52} *tp53*-null zebrafish is similar compared to *rabl3* wild-type *tp53*-null siblings (Fig. 2d). In the *tp53* wild-type background, mutant *rabl3-TR*^{52} alone did not cause tumor formation within 14 months, consistent with a requirement for a second insult. (2) To confirm that the impact of Rabl3-TR is not specific to a *tp53*-null background, a chemical carcinogenesis model was used: zebrafish were sensitized to tumor development by exposure to the carcinogen 7,12-dimethylbenz[a]anthracene (DMBA)[6]. Heterozygous *rabl3-TR*^{41} mutants develop tumors at almost twice the rate of their *rabl3* wild-type siblings, including cholangiocarcinoma and hepatocellular carcinoma (Fig. 2e–g and Supplementary Fig. 1b; $N = 57$, $P = 0.0149$). These findings corroborate the role of the mutant *RABL3* allele in promoting cancer susceptibility in a vertebrate model.

The biological function of RABL3 is largely unknown. A prior study of RABL3 function found that overexpression enhanced cell proliferation and motility, whereas knockdown increased apoptosis in breast cancer cell lines, which is suggestive of an oncogene function[7]. To identify the role of RABL3 and the mechanism by which the mutant allele promotes

cancer, we performed transcriptional profiling of wild-type and homozygous *rabl3-TR*[41] larval zebrafish at 21 days of age, before the occurrence of any tumors, revealing a large number of differentially expressed genes (Supplementary Fig. 2). Gene-set enrichment analysis uncovered a signature for activation of KRAS pathway signaling (Supplementary Fig. 2). Indeed, RABL3_p.Ser36* expression augments RAS signaling in the context of human pancreatic duct epithelial cells (Supplementary Fig. 3). To gain mechanistic insight into the action of RABL3, we performed affinity purification–mass spectrometry (AP–MS) of stably expressed tagged RABL3 and RABL3_p.Ser36* and used the Comparative Proteomics Analysis Software Suite (CompPASS) to identify high-confidence interacting proteins (HCIPs)[8]. AP– MS of RABL3 or RABL3_p.Ser36*-tagged baits from HEK293T cells revealed a number of HCIPs, including Rap1 GTPase-GDP dissociation stimulator 1 (RAP1GDS1, SmgGDS) (Fig. 3a and Supplementary Table 1). Surprisingly, RABL3_p.Ser36* interacted with RAP1GDS1 with higher affinity as determined by the normalized weighted D (NWD) score and the number of normalized RAP1GDS1 assembled peptide spectral matches (APSMs) identified in RABL3 versus RABL3_p.Ser36* AP–MS experiments (Fig. 3b and Supplementary Table 1; $P = 0.0014$). These interactome data suggest that the truncated protein may be functional, which is supported by molecular dynamic simulations predicting that RABL3_p.Ser36* can maintain a stable secondary structure of a β-strand and an α-helix (Supplementary Fig. 4a–d), as well as by purification of recombinant RABL3_pSer36* (Supplementary Fig. 5). Moreover, mass spectrometry parallel reaction monitoring (PRM) analysis is consistent with the presence of the truncated Rabl3 in vivo in the heterozygous mutant but not in wild-type zebrafish (Supplementary Fig. 6). To confirm that RABL3_p.Ser36* interacts with RAP1GDS1, we immunoprecipitated RABL3_p.Ser36* from transfected HEK293T cells, and detected two splice variants, RAP1GDS1–607 and RAP1GDS1–558 (ref. [9]) (Supplementary Fig. 7a). RAP1GDS1, also known as SmgGDS, is a chaperone thought to bind small GTPases and regulate their prenylation, a lipid posttranslational modification required for the activity of many oncogenic proteins including KRAS[3,9–12]. Indeed, immunoprecipitation of RABL3_p.Ser36* pulls down both RAP1GDS1 and KRAS as binding partners, indicative of a trimeric complex (Supplementary Fig. 7b). These unbiased transcriptomic and proteomic approaches independently implicate RABL3 as a potential regulator of KRAS signaling. Consistent with a pathway interaction, we identified a noticeable correlation between *RABL3* and *KRAS* transcript abundance in multiple TCGA cohorts (Supplementary Fig. 8).

Aberrant KRAS signaling is found in the vast majority of pancreatic cancers[13,14]. Therefore, given its direct interaction with RAP1GDS1, we postulated that RABL3_p.Ser36* impacts KRAS prenylation. To test this hypothesis, the effects of RABL3_p.Ser36* on KRAS-4B prenylation kinetics were examined using an established mevastatin block-and-release assay[11]. RABL3_p.Ser36* significantly increases prenylation rates of both KRAS-4B and oncogenic KRAS-4B (G12V) (Fig. 3c,d; $P < 0.05$). Consistent with an impact on KRAS prenylation, RABL3_p.Ser36* enhances the trafficking of KRAS to the plasma membrane (Supplementary Fig. 9). To test whether the impacts of RABL3_p.Ser36* are KRAS-dependent, RABL3_p.Ser36* was expressed in $KRas^{lox}$ mouse embryonic fibroblasts (MEFs) carrying null *HRas* and *NRas* alleles and a floxed but functional *KRas* locus ($HRas^{-/-}; NRas^{-/-}; KRas^{lox/lox}; RERTn^{ert/ert}$ MEFs), or in *RASless* MEFs in which *KRas* alleles

have been excised (*HRas*$^{-/-}$; *NRas*$^{-/-}$; *KRas*$^{-/-}$;*RERTn*$^{ert/ert}$ MEFs)[15] (Supplementary Fig. 10). Whereas RABL3_p.Ser36* was sufficient to augment proliferation in *KRas*^{lox} MEFs, this impact was lost in *RASless* MEFs (Fig. 3e), supporting a mechanism for RABL3_p.Ser36* acting through RAS proteins. Moreover, when prenylation is blocked in the presence of mevastatin, the impacts of RABL3_p.Ser36* on cell proliferation are lost (Supplementary Fig. 11). Taken together, it is intriguing to speculate that RABL3_p.Ser36* can promote cancer at least in part by interaction with RAP1GDS1 and subsequent alteration in the prenylation rate of small GTPases including KRAS (Fig. 3f). We have not ruled out additional possible impacts of RABL3_p.Ser36* on other small GTPases.

Germline mutations that dysregulate the RAS pathway have not only been associated with cancer, but also with a spectrum of craniofacial dysmorphologies, short stature, neurocognitive impairments and other phenotypic consequences that are collectively termed RASopathies[16]. Having found that Rabl3-TR dysregulates Ras activity and confers cancer susceptibility in heterozygous zebrafish carriers, we investigated the phenotypic consequences in homozygous mutant Rabl3-TR zebrafish. A survey of somites, heart, pancreas, liver and hindbrain markers revealed no overt abnormalities in homozygous mutant embryos (Supplementary Fig. 12). While having a normal body length as larvae, homozygous mutants exhibited progressively stunted growth as early as 3 weeks postfertilization (Fig. 4a), and severe kyphosis and dysmorphic craniofacial and rib bones by 12 weeks postfertilization (Fig. 4b). Adult homozygous mutants manifested swimming defects suggestive of neurologic or motor abnormalities (Supplementary Video 1). Analysis of cranio facial structures by three-dimensional (3D) micro-computed tomography (μCT) revealed severely impaired bone mineralization (Fig. 4b–f). These defects bear a striking resemblance to stunted growth and skeletal abnormalities observed in patients with RASopathies, as well as in mice with dysregulated Ras signaling[17,18], which suggests that the observed phenotype in homozygous *rabl3* mutants may be mechanistically related to these disorders. To test the functional importance of dysregulated Ras signaling for the observed phenotypes, homozygous *rabl3-TR*^{41} mutant zebrafish were raised in the presence of the MEK inhibitor trametinib. Longterm MEK inhibition resulted in a partial rescue in skeletal mineralization (Fig. 4e–g Supplementary Fig. 13), body length (Fig. 4h) and swimming behavior (Supplementary Videos 1–3) of homozygous *rabl3-TR*^{41} mutant zebrafish. These findings, corresponding to the rescue effects of MEK inhibition in *KRas*^{V14I} mutant mice[18], support the role of dysregulated Ras signaling in the phenotypes of homozygous *rabl3* mutant zebrafish and demonstrate a therapeutic strategy for affected patients.

Here, we found a germline mutation not previously associated with hereditary cancer and directly validated its impact on cancer formation in vivo using zebrafish. We anticipate this strategy will be widely applicable for high-throughput classification of variants in other candidate genes, as well as a growing list of existing variants of uncertain significance in established cancer risk genes. The *RABL3_p.Ser36** mutation was identified in a family with a high incidence of PDAC and other cancers. Therefore, like other causative germline mutations in established familial PDAC genes, the *RABL3_p.Ser36** mutation probably predisposes to cancer in other organs. The mechanisms dictating specificity for the pancreas or other organs for these genetic etiologies in cancer have not been elucidated.

The *RABL3_p.Ser36** allele is rare in the general population and is probably a recent occurrence in the family sequenced here, consistent with its robust cancer association. Testing for this and, potentially, other mutations in *RABL3* may reveal the genetic predisposition and help prognosticate risk in other families with an unsolved hereditary cancer syndrome. While a recent genomic survey of 638 patients with familial PDAC revealed 6,114 premature truncating variants in 4,553 genes[19], this knowledge can only lead to clinically relevant insight after in-depth functional and mechanistic analysis. More broadly, our findings uncover a mechanism by which RAS pathway signaling may be regulated in both hereditary and sporadic cancer, and brings attention to a gene that has not been identified by somatic mutation analysis of PDAC. RABL3 and related RAB proteins were hits in a recent screen for genes that affect AKT phosphorylation and that may have rare driver mutations in sporadic cancer, and which have not been previously discerned by statistical analysis of somatic mutations[20]. Notably, RABL3 appears to have mutational hotspots in human tumor sequence databases, and these residues colocalize to the predicted interface with RAP1GDS1, suggesting a potential driver role in cancer (Supplementary Fig. 14 and Supplementary Table 2). Remarkably, germline mutations in these same residues have a statistically significant burden among 8,600 individuals with congenital, developmental and/or neurologic disorders referred for clinical exome sequencing (R157C: $P = 5.7 \times 10^{-5}$; R184Q: $P = 0.04$; Supplementary Table 3; phenotypes detailed in Supplementary Table 4), which is consistent with a biologically important role for RABL3 during development. Furthermore, we find a striking enrichment of the germline RABL3_p.Arg184Gln variant in TCGA exomes ascertained from individuals with cancer versus those in the non-TCGA ExAC cohort ($P = 0.0074$; Supplementary Table 5), which is consistent with cancer susceptibility conferred by this germline variant. Indeed, in a second family with a history of five relatives with PDAC but unrevealing panel genetic testing, we identified the heterozygous germline *RABL3_p.Arg184Gln* variant in three affected relatives (Supplementary Fig. 15). We compared the impact of these additional RABL3 variants to RABL3_p.Ser36* in two complementary assays: (1) cell proliferation in vitro and (2) zebrafish gastrulation in vivo, an embryonic process that has been established as a sensitive and quantitative readout of RAS pathway dysregulation[21]. Similar to RABL3_p.Ser36*, RABL3_p.Arg157Cys augments cell proliferation of HEK293T cells and disturbs zebrafish gastrulation consistent with RAS pathway activation, whereas RABL3_p. Arg184Gln does not (Supplementary Figs. 16 and 17), suggesting diverse mechanisms by which RABL3 mutations may impact cancer risk. Given the association of these RABL3 germline or somatic variants with cancer, we examined multiple PDAC cell lines and found a strikingly elevated level of RABL3 expression (Supplementary Fig. 18), which is consistent with a driver role in cancer and a role in regulating KRAS trafficking. Indeed, overexpression of RABL3 is sufficient to promote cell proliferation (Supplementary Fig. 16), alter zebrafish gastrulation (Supplementary Fig. 17) and impact prenylation (Supplementary Fig. 19). Moreover, *RABL3* knockdown abrogates proliferation in PDAC cells, indicating a requirement for RABL3 in the proliferation of these cancer lines (Supplementary Fig. 18). Put together, these findings are consistent with our observations in *rabl3* mutant zebrafish and suggest a broader critical role for RABL3 in both development and cancer. We postulate that the interaction between RABL3 and RAP1GDS1 may serve an important role in

regulating the intracellular processing of KRAS and other GTPases, and therein may offer an attractive therapeutic target for altering RAS pathway activity in cancer.

Methods

WGS and computational analysis of a human family.

WGS was performed on Illumina HiSeq 2000. Genomic DNA was isolated from blood samples, randomly fragmented and then sequenced using 100-base pair paired-end reads to achieve approximately 31× mean genomic coverage per library. Two independent libraries were produced and sequenced for one of the individuals to lower the likelihood of PCR artifacts in variant discovery. Our computational pipeline performs fast, highly parallelized sequencing analysis from raw reads to assessment of shared rare variation[4]. The output paired-end FASTQ files from the sequencer were aligned to the human reference sequence (University of California Santa Cruz hg19 build) using the Burroughs–Wheeler alignment tool[22] in paired-end mode followed by base quality recalibration and targeted local realignment focused around known short insertions and deletions (indels) using the Genome Analysis Toolkit (GATK)[23]. Duplicated reads from sequencing the same DNA fragment were discarded. Single nucleotide substitutions and indels were identified for both samples simultaneously using the Unified Genotyper tool from the GATK in multisample calling mode. Variant quality score recalibration was performed using the GATK to identify a set of high-confidence variants.

WGS generated 5.86 million single nucleotide variants (SNVs) per genome (~46,000 SNVs per exome) in total amongst the two family members. We applied the following filters to narrow the pool of candidate variants: (1) variants that are rare (minor allele fraction, MAF < 0.1% in the ExAC database, Exome Sequencing Project or 1000 Genomes Project data); (2) variants present in both affected family members; (3) variants that were heterozygous; (4) protein-altering variants; (5) variants not present in a panel of unrelated normal genomes to account for common sequencing artifacts. The numbers of SNVs obtained by these filters are shown in Fig. 1b. Further manual review of sequencing data and interpretation was applied to produce a list of candidate causative variants.

Consent to perform WGS under Clinical Laboratory Improvement Amendments conditions was obtained under protocols approved by the Institutional Review Board (IRB) of Dana-Farber Cancer Institute. Explicit consent was obtained from the family to publish these findings and the family pedigree.

Zebrafish husbandry.

Zebrafish were maintained according to Institutional Animal Care and Use Committee (HMS IACUC 04626) protocols. Lines used in this study include wild type (Tübingen) and *tp53*$^{-/-}$ (ref. [5]).

CRISPR–Cas9 genome editing.

The zebrafish *rabl3* genome sequence was targeted using the guide RNA (gRNA) 5′-GGGGAATCCCTCATGGACTGTGG-3′, a gRNA that is predicted to have no off-target

sites assuming up to two mismatches (https://chopchop.rc.fas.harvard.edu). The gRNA template was generated by annealing an oligonucleotide containing the T7 (5′-TAATACGACTCACTATA-3′) promoter sequence and the gRNA sequence was annealed to an oligonucleotide encoding the reverse complement of the tracrRNA tail. A double-stranded DNA (dsDNA) template was generated by filling in the single-stranded DNA (ssDNA) overhangs using T4 DNA polymerase (NEB), the template was purified, and the gRNA was synthesized by transcription using the MEGAshortscript T7 kit (Ambion) and purified by ammonium acetate precipitation. A zebrafish codon-optimized version (zCas9) of the *Streptococcus pyogenes* Cas9 mRNA with SV40 large T antigen nuclear localization signals (nls) was generated by in vitro transcription from a pT3TS-nls-zCas9-nls plasmid template (gift of S. Wente, Vanderbilt University) and purified using the RNeasy Mini Kit (Qiagen). Zebrafish (Tübingen background) zygotes were injected in the single cell with 1 nl of a mix of 150 ng μl^{-1} zCas9 mRNA + 50 ng μl^{-1} gRNA + 0.2 M KCl + Phenol Red dye. Mutagenesis rates were determined by PCR of the targeted region (forward primer: 5′-TGGCTACCACATCATAGCTGA-3′, 248 nucleotides upstream of the gRNA; reverse primer: 5′- GCCAACAGATCCTCCAACAT-3′, 179 nucleotides downstream of the gRNA) followed by TOPO TA cloning (Invitrogen) and sequencing of individual clones. Mutagenesis efficiency was first confirmed by screening of injected F_0 embryos; subsequently injected F_0 zebrafish were raised to adulthood and outcrossed, and F_1 embryos were screened for *Rabl3* mutations. Founders carrying each *Rabl3* mutant allele were established in the F_1 generation, and tumor studies were performed in the F_3 or later generations. Identification of carriers in F_2 or later generations was facilitated by restriction-fragment length polymorphism analysis following digestion with HpyCH4III (NEB) at the *rabl3* mutation site.

Zebrafish tumor studies.

For spontaneous tumor formation in a *tp53* mutant background, *tp53*$^{-/-}$ and *tp53*$^{-/-}$;*rabl3-TR*^{52} siblings were raised until 8 weeks postfertilization, at which point they were genotyped at the *rabl3* locus and then allocated to a density of six zebrafish per tank to facilitate tumor monitoring and ensure uniform husbandry and feeding conditions. Fish were monitored three times per week for tumor formation over the subsequent 12 months. Once tumor growth was observed in a fish, the fish was isolated to confirm the growth and then euthanized, dissected and the histology was examined in a blinded fashion by a zebrafish pathologist (J.R.H.) to confirm and characterize the tumor.

For DMBA-induced carcinogenesis, wild-type and heterozygous *rabl3-TR*^{41} siblings were raised and then exposed at 3, 4 and 5 weeks postfertilization to DMBA at 5 ppm for 24 h for each exposure, as previously described[6,24].

The following day, fish were rinsed several times, then allowed to recover in isolated tanks in the dark for 24 h, then returned to the system aquarium tanks. Fish were monitored three times per week for tumor formation over the subsequent 4 months. Once tumor growth was observed in a fish, the fish was isolated to confirm the growth and then euthanized, dissected and the histology was examined in a blinded fashion by a zebrafish pathologist (J.R.H.) to confirm and characterize the tumor. Deceased fish were collected, genotyped and sent for

necropsy and histological analysis to evaluate for the presence of occult tumors. At 18 weeks postfertilization, all the remaining fish were euthanized, genotyped, dissected and sent for blinded histological analysis (J.R.H.).

While the effect size of the *rabl3-TR* heterozygous allele in these zebrafish cancer models was initially unknown, we estimated a total sample size of $N = 55$ per group based on a hazard ratio of 4, overall probability of cancer at 30%, a power of 0.8 and a type I error rate of 5% using a Cox two-sided proportional hazards model.

Histology, in situ hybridization and immunohistochemistry.

Zebrafish embryos were fixed in paraformaldehyde and processed for in situ hybridization using standard protocols (http://zfin.org/ZFIN/Methods/ThisseProtocol.html). Adult zebrafish were fixed in Dietrich's fixative, paraffin-embedded and serially sectioned at 5–10 μm and stained with hematoxylin and eosin (H&E) using standard techniques. For immunohistochemistry, fixed tissue was embedded in paraffin and serially sectioned for H&E and immunohistochemical analysis. Slides were deparaffinized and rehydrated prior to heat-induced antigen retrieval. Cholangiocarcinoma was visualized using a primary antibody (2F11; Abcam, ab71286) and processed using an HRP/DAB (ABC) detection kit (Abcam, ab64264).

Zebrafish RNA-seq.

RNA was extracted using TRIzol reagent (Life Technologies) from wild-type and *rabl3-TR*[41] larval zebrafish at 3 weeks postfertilization according to the manufacturer's instructions. RNA quality was checked by Agilent Bioanalyzer. Sequencing was performed after library construction on an Illumina HiSeq. Paired-end reads were aligned using Star v.2.3 to the zebrafish genome (Zv9). The mapped reads were counted using HTSeq-count (v.0.6.0) and gene models from Ensembl transcriptome. Analysis of differential gene expression was performed using DESeq2 (ref. [25]). Orthology to human genes was determined using Ensembl and supplemented by performing BLAST. Gene-set enrichment analysis[24] was performed using normalized counts.

Interaction proteomics and MS analysis.

Interaction proteomics was performed as described previously[8,26]. Briefly, HEK293T cells were transduced with a lentiviral vector expressing amino (N)-terminal or carboxy (C)-terminal hemagglutinin (HA)-FLAG-tagged RABL3, C-terminal HA-FLAG RABL3_p.Ser36* or C-terminal HA-FLAG-tagged RAP1GDS1, and stable cell lines were selected with puromycin. HEK293T cells from 4 × 15 cm^2 dishes were collected for anti-FLAG AP–MS studies in biological duplicate (RABL3 both N-terminal and C-terminal tagged, RAP1GDS1) and triplicate (RABL3_p.Ser36*). The biological replicates were processed as follows. Cells were lysed in 3 ml of 50 mM Tris–HCl (pH 7.4), 150 mM NaCl, 0.5% Nonidet P40, 1 mM dithiothreitol and protease and phosphatase inhibitors. Clarified lysates were filtered through 0.45-μm spin filters (Millipore Ultrafree-CL) and immunoprecipitated with 60 μl anti-FLAG magnetic beads per replicate (Sigma). Complexes were washed four times with lysis buffer and three times with PBS and eluted with FLAG peptide at room temperature. Elutions were carboxymethylated by reduction and precipitated

with trichloroacteic acid. Trichloroacteic acid-precipitated proteins were trypsinized, purified with Empore C18 extraction media (3M) and analyzed using liquid chromotography– tandem mass spectrometry (LC–MS/MS) with a LTQ-Velos linear ion trap mass spectrometer (Thermo) with an 18 cm^3, 125 μm (internal diameter) C18 column and a 50-min 8–26% acetonitrile gradient. Complexes were analyzed twice by LC–MS to generate technical duplicates. Spectra were searched with Sequest against a target–decoy human tryptic UNIPROT-based peptide database, and these results were loaded into CompPASS[8,26] to identify HCIPs. Individual experiments were analyzed using a statistics table derived from analogous AP–MS data for 48 unrelated proteins, to determine NWD scores and *Z*-scores based on spectral counts. To identify bait-associated proteins, proteins were filtered at a 2% false discovery rate for those with a NWD score ≥1.0 and APSMs ≥2 (Supplementary Table 1). HCIPs for the RABL3_p.Ser36* AP–MS experiments were determined from the overlap of all three biological replicates. RABL3 HCIPs were determined using the overlap from both N-terminal and C-terminal HA-FLAG replicates, as well as information available from similar AP–MS experiments from Huttlin et al. deposited in BioGrid[27]. Likewise, for RAP1GDS1, HCIPs were determined using the overlap of biological replicates and data from Huttlin et al. deposited in BioGrid[27]. This list of HCIPs was used to generate interaction maps using Cytoscape. For clarity, only small GTPases that interact with RAP1GDS1 were displayed in the Cytoscape map and grouped according to protein family. To determine RAP1GDS1 bait-normalized APSMs for AP–MS with either RABL3 or RABL3_p.Ser36* (Fig. 3b), RABL3 peptides in common between the two baits (specifically: $_7$VKVLVLGDSGVGK$_{19}$ and $_9$VLVLGDSGVGK$_{19}$) were tabulated for each of three biological replicates (RABL3_p.Ser36* AP–MS experiments) and four biological replicates (RABL3 AP–MS). Average RABL3 APSMs across AP–MS experiments were calculated and then used to normalize the RAP1GDS1 APSMs in RABL3 versus RABL3_p.Ser36* AP–MS experiments. The processed proteomics data reported in this paper are available in Supplementary Table 1 and RAW files are available at Peptide Atlas under accession number PASS01355.

MS PRM assay.

A PRM assay[28] was used to examine the tryptic peptides prepared from total protein obtained from intestine, pancreas and liver organs dissected from adult wild-type and *rabl3-TR*$^{41/+}$ heterozygous mutant zebrafish. The digested proteins were subjected to tandem LC–MS/MS analysis at the Proteomic Core Facility at the Children's Hospital of Philadelphia. Briefly, a nanoflow, ultra-high performance LC instrument (Dionex UltiMate 3000, ThermoFisher Scientific) was coupled online to a Q-Exactive HF MS (ThermoFisher Scientific) with an EasySpray ion source (ThermoFisher Scientific). Reverse-phase chromatography was performed with a binary buffer system consisting of HPLC grade water plus 0.1% formic acid (solvent A) and 100% acetonitrite with 0.1% formic acid (solvent B) with a flow rate of 300 nl min^{-1}. Samples were first loaded onto a trap column (Acclaim PepMap 100, 3 μm, 75 μm internal diameter × 2 cm nanoViper, ThermoFisher Scientific) and injected via a C18 analytical column (PepMap RSLC, 2 μm, 75 μm internal diameter × 50 cm packed tip column, ThermoFisher Scientific). For ionization, 1.8 kV of liquid junction voltage and 275°C capillary temperature were used. The peptides were separated using a 150-min gradient. The Q-Exactive HF MS was operated in the targeted MS/MS

mode using Xcalibur software. The acquisition method combined a full-scan method with a time-scheduled and unscheduled sequence, using 4.0 *m*/*z* individual isolation windows. The target ion value was set at 1×10^5, and maximum ion fill time was 100 ms. Fragmentation was performed with a normalized collision energy of 27% and MS/MS scans were acquired with an orbitrap resolution of 15,000 at *m*/*z* 200. A synthesized peptide (Anaspec Peptide) was used to generate the spectral library for the RABL3 wild-type and Ser36* mutant tryptic peptides. The data were processed using MaxQuant and the identified MS/MS spectra were used to build the spectral library for accurate interpretation of PRM analysis. Data analyses were performed using Skyline daily[29] (v.4.1.1.18118). Integrated peaks were manually inspected to ensure correct peak detection and integration.

Protein structure simulations.

The protein model for RABL3 was created with YASARA homology modeling[30] and that for RABL3_p.Ser36* with QUARK ab initio modeling[31]. Molecular dynamics of RABL3 were performed in YASARA using the GPU-enhanced AMBER03 force field for 350 ns. Docking of proteins was performed using ZDOCK[32] followed by energy minimizations of the interactions in the YASARA2 force field and AMBER03, with the addition of a water shell.

Human cell culture and transfection.

HEK293T cells (HEK293T/17, American Type Culture Collection (ATCC) CRL11268) were cultured in DMEM media supplemented with 10% heat-inactivated fetal bovine serum and antibiotics. The complementary DNAs encoding RAP1GDS1–558 or RAP1GDS1–607 were generated as previously described[9], and the cDNAs encoding myc-tagged small GTPases were purchased from the cDNA Resource Center (www.cDNA.org). All cDNAs were transfected into cells using Lipofectamine 2000 (Invitrogen) according to the manufacturer's protocol. Relative levels of HA-tagged RABL3 proteins expressed in cells were quantified by western blot (16B12, Covance, catalog no. MMS-101P) followed by densitometry, revealing a 50-fold greater level of expression of the full-length RABL3 protein compared with the truncated RABL3_p.Ser36* protein. For immunoprecipitation studies examining the interaction of RABL3 variants with RAP1GDS1, cells were transfected with cDNA encoding RAP1GDS1–558 to improve detection of this splice variant along with the far more abundant and prominently visible RAP1GDS1–607 splice variant, as established previously[9]. The relative abundance of RAP1GDS1–607 compared with RAP1GDS1–558 is observed in multiple cell lines, and transfection with cDNA encoding RAP1GDS1–558 does not alter the interaction of RABL3_p.Ser36* with RAP1GDS1–607. For human cell proliferation studies, HEK293T cells were plated in a 10-cm dish at a concentration of 3×10^6 cells per dish. After culturing for 18–24 h, the cells were transfected with 4 μg of the indicated cDNA using Lipofectamine 2000 (Invitrogen, Life Technologies). At 17–20 h post-transfection, the cells were plated in 96-well plates at a concentration of 3×10^3 cells per well. The cells were allowed to settle at 37°C for 4–5 h before being placed into an Incucyte Zoom reader (Essen Bioscience). Readings were taken for the indicated times.

The following cell lines were obtained from the ATCC (https://www.atcc.org): HPAC, SW1990, PL45, HPAF-II, PANC-1, Panc 02.03, Panc 10.05, BxPC-3 and Capan-2. The following cell lines were obtained from the German Collection of Microorganisms and Cell Cultures (https://www.dsmz.de/catalogues/details/culture): PA-TU-8988T, PA-TU-8988S, PA-TU-8902 and DAN-G. The following cell lines were obtained from Sigma-Aldrich: HuP-T3, HuP-T4 and AsPC-1. Cell lines were authenticated by fingerprinting as well as visual inspection and carefully maintained in a centralized cell bank. All cell lines were tested routinely, and before all experiments, for mycoplasma contamination. Cell lines were cultured in DMEM (Invitrogen, catalog no. 11965) with 10% fetal bovine serum and 1% penicillin– streptomycin except for human pancreatic ductal epithelial cells (HPDE), which have been previously described and were grown as indicated[33]. The following antibodies were used for the RAS pulldown assay and western blot analysis of HPDE cells: RAS (Upstate, catalog no. 05–516), P-ERK (Cell Signaling, catalog no. 4370), ERK (Cell Signaling, catalog no. 9102), Actin (Sigma-Aldrich, catalog no. A2066), KRAS (Santa Cruz, catalog no. sc-30), Vinculin (Cell Signaling, catalog no. 4650), hemagglutinin (Covance, catalog no. MMS-101P).

KRAS intracellular localization experiments.

HEK293T cells were plated at a density of 0.9×10^4 cells ml^{-1} on uncoated glass coverslips in each well of a 24well plate, and cultured for 3 d at 37 °C and 5% CO_2. Cells were transfected with pcDNA3.1-Myc-WT-KRAS and cotransfected with either pcDNA3.1-RABL3_p. Ser36*-HA or pcDNA3.1-HA vector using Lipofectamine 2000 (Life Technologies). At 2.5 h after transfection, the cells were fixed in 3% formaldehyde in PBS, and autofluorescence due to formaldehyde was quenched with 50 mM NH_4Cl in PBS. Cell membranes were permeabilized with 0.2% Triton-X-100, and nonspecific protein-binding sites were blocked with 1% BSA in PBS. Cells were stained with c-Myc antibody (9E10, Santa Cruz Biotechnology) conjugated to Alexa Fluor 488 (Santa Cruz Biotechnology) and with HA antibody (16B12, BioLegend) conjugated to Alexa Fluor 568 (Molecular Probes), and nuclei were stained with DAPI. Cells were imaged using a Nikon Eclipse Ni-U fluorescence microscope and images captured using Nikon Elements software. Images were processed to correct for uneven illuminated background fluorescence using the 'rolling ball' algorithm in Fiji with a radius of 10.0 pixels. To quantify distribution of KRAS in an individual cell, an 8-μm line (10 pixels wide) was drawn in Fiji between two edges of plasma membrane, spanning cytoplasm but not nucleus, as guided by DAPI staining. The fluorescence intensity along this 8-μm line, spanning plasma membrane–cytoplasm–plasma membrane, was quantified at 120 points along this line. Localization of KRAS was quantified in >15 individual cells for each condition from three independent experiments.

RASless MEF experiments.

KRas^{lox} MEFs (line DU1473) were obtained from the National Cancer Institute and cultured as previously described[15]. RASless MEFs were generated by addition of 600 nM 4-hydroxytamoxifen (4-OHT, Sigma-Aldrich) to media and replacement of fresh media with 4-OHT every 2–3 d for 14 d total. MEFs were then transduced with lentiviral constructs for RABL3_p.Ser36* or vector control, selected with blasticidin for 10 d until all uninfected MEFs were dead, and then plated for proliferation studies at a density of 10×10^3 cells per

well in 6-well dishes, with triplicates of each condition and each time point. Western blot analysis of MEFs was performed at the beginning and end of the proliferation studies to confirm the presence of RABL3_p.Ser36*-HA by hemagglutinin tag (16B12, Covance, catalog no. MMS-101P), KRas (F234, Santa Cruz, catalog no. sc-30), pERK1/2 Thr 202/Thr 204 (Cell Signaling, catalog no. 4370) and vinculin as loading control (Cell Signaling, catalog no. 4650).

Immunoprecipitation and enhanced chemiluminescence immunoblotting.

Immunoprecipitation and enhanced chemiluminescence immunoblotting were conducted as previously described[9]. The following antibodies were used: anti-Rap1GDS1 (rabbit polyclonal; ProteinTech, catalog no. 10377-1-AP) (validation at http://www.antibodypedia.com/gene/6907/RAP1GDS1/antibody/151922/103771-APanti-Rap1GDS1); anti-Rap1GDS1 (mouse monoclonal; Santa Cruz, catalog no. sc-390003 (clone F-1)) (validation at http://www.scbt.com/datasheet-390003rap1gds1-f-1-antibody.html); anti-myc (rabbit; Biolegend, catalog no. 906302 (clone poly9063)) (validation at http://www.biolegend.com/pop_pdf.php?id=11327, described in Berg et al.[9]); anti-myc (mouse; Santa Cruz, catalog no. sc-40 (clone 9E10)) (validation at http://datasheets.scbt.com/sc-40.pdf, described in Berg et al.[9]); anti-HA.11 (rabbit; Biolegend, catalog no. 902302 (clone poly9023)) (validation at http://www.biolegend.com/pop_pdf.php?id=11375, described in Berg et al.[9]); anti-HA.11 (mouse; Biolegend, catalog no. 901503 (clone 16B12)) (validation at http://www.biolegend.com/pop_pdf.php?id=11374, described in Berg et al).[9]

Prenylation block-and-release assay.

A previously described technique[11] was used to assess the rate of KRAS-4B prenylation. HEK293T cells were transfected with the indicated cDNAs, and 90 min later exposed to mevastatin (10 μM). After 24 h, the mevastatin was removed by washing and the cells were placed in fresh media. The cells were collected at different time points after the removal of mevastatin, and lysed in laemmli sample buffer. The samples were immunoblotted using myc antibody to detect the expressed myc-tagged KRAS-4B or KRAS-4B (G12V) proteins. The relative amount of prenylated and nonprenylated proteins was determined by calculating the optical densities of the proteins in immunoblots using digital imaging (ImageQuant LAS 4000 digital imager, GE Healthcare Systems).

Zebrafish trametinib rescue studies.

Zebrafish larvae from a cross of heterozygous *rabl3-TR*[41] mutant parents were raised per routine until 10 d postfertilization, at which time they were divided into vehicle control or trametinib treatment cohorts. Cohorts were raised in subgroups of 25 larvae per tank. Five times per week, cohorts were treated for 12–16 h overnight with 0.1 μM trametinib (LC Laboratories, T-8123) or equivalent volume of DMSO (final percentage 0.1%) in 500 ml fresh fish water per tank. In the morning, water was replaced with 1 l fresh fish water and fish were fed with standard nursery diet of spirulina and hatchfry.

Zebrafish skeletal analysis.

For μCT analysis, a Scanco Medical μCT 35 system with an isotropic voxel size of 7 μm was used. Scans were conducted in euthanized fish in 70% ethanol and used an X-ray tube potential of 55 kV, an X-ray intensity of 0.145 mA and an integration time of 600 ms.

For analysis of vertebrae of 3-month-old zebrafish, 20 slices, with a slice increment of 5 μm, of the first cervical vertebrae were contoured with a threshold for 250 mgHA cm^{-3} or 200 mgHA cm^{-3}. For analysis of parietal bone, a region of 50 slices was analyzed with the same parameters. Gaussian filter values with a sigma value of 0.8 and support value of 1 were used throughout. 3D images were obtained from contoured two-dimensional images by methods based on distance transformation of the binarized images. All images presented are representative of the respective genotypes.

For bone histology, skeletons were fixed in 4% paraformaldehyde for 24–36 h before decalcification with 10% tetrasodium EDTA overnight. Tissues were dehydrated by passage through an ethanol series, cleared twice in xylene, embedded in paraffin and sectioned at 7-μm thickness along the sagittal plane.

Alizarin Red staining was performed using standard protocols.

Somatic variation in human cancers.

A multi-species sequence alignment of RABL3 for 131 species was compared with the same alignment of ten other small GTPases. This conservation analysis revealed a set of amino acids that are conserved in RABL3 and seen in other small GTPases, and also revealed a set of variants that are conserved but unique to RABL3 (Supplementary Fig. 14). These highly conserved variant sites that were unique to RABL3 were screened for recurrent cancer missense variants in the cBioPortal (https://www.cbioportal.org/, accessed 24 August 2016).

Germline associations in developmental patients and TCGA samples.

Using the set of RABL3 variants that were identified as recurrent somatic mutations in cancer (Supplementary Fig. 14), each variant was screened for germline mutations in a set of 8,600 individuals with congenital, developmental and/or neurologic disorders referred for clinical exome sequencing at the Baylor College of Medicine, and used as the basis for a hypergeometric association test (Supplementary Tables 3 and 5). For each allele, we adjusted the expected allele counts using population demographic data in ExAC, but the burden was statistically significant with and without this adjustment.

Separately, we compared the presence of each highly conserved variant in a set of germline samples associated with cancer cases from TCGA in ExAC (N = 7,601 individuals) with non-TCGA samples from ExAC (N = 53,105 individuals). For each variant, we screened for significant associations in the TCGA germline samples over all ExAC samples, using a hypergeometric test. Comparisons were performed for the subset of non-Finnish Europeans as well as the complete ExAC dataset.

Statistical analysis.

Statistical tests and results are indicated within the figure legends. Data are depicted as mean ± s.e.m. unless otherwise indicated. Adult zebrafish Kaplan–Meier tumor-free survival curves were analyzed by log-rank Mantel–Cox test. Body length comparisons for adult zebrafish were analyzed by unpaired two-tailed *t*-test. The impact of trametinib on bone histomorphometric quantification was analyzed by unpaired one-tailed *t*-test. Associations of germline RABL3 variants with cancer or with congenital, developmental and/or neurological disorders were analyzed by a hypergeometric distribution test. Impacts of RABL3 variants on cell proliferation were analyzed by unpaired *t*-test corrected for multiple comparisons using the Holm–Sidak method. Pairwise comparisons of the impact of various *RABL3* mutant alleles on zebrafish gastrulation were analyzed by a Kruskal–Wallis multiple comparisons test with Dunn's correction.

Reporting Summary.

Further information on research design is available in the Nature Research Reporting Summary linked to this article.

Supplementary Material

Refer to Web version on PubMed Central for supplementary material.

Acknowledgements

This work was supported by the NIH grant nos. K08 DK105326 (to S.N.); R01 DK090311, R01 DK095721 and R24 OD017870 (to W.G.); R01 GM095567, R01 CA157490, R01 CA188048, P01 CA117969 and R35 CA232124 (to A.C.K.); R01 CA188871 (to C.W.) and R01 GM040602 (to C.A.F.); as well as grants from the National Pancreas Foundation (to S.N.), the Harvard Digestive Diseases Center (grant no. P30 DK034854 to S.N. and W.G.), the Ken and Louise Goldberg Award (to S.N.), an ACS Research Scholar Grant (RSG-13-298-01-TBG to A.C.K.), the Lustgarten Foundation and SU2C (to A.C.K) and the Anna Fuller Fund and the Claudia Adams Barr Program for Innovative Cancer Research (to W.G.). S.N. is a recipient of the Burroughs Wellcome Fund Career Award for Medical Scientists. W.G. is a Pew Scholar in the Biomedical Sciences.

Competing interests

A.C.K. has financial interests in Vescor Therapeutics, LLC. A.C.K. is an inventor on patents pertaining to Kras-regulated metabolic pathways, redox control pathways in pancreatic cancer, targeting GOT1 as a therapeutic approach and the autophagic control of iron metabolism. A.C.K. is on the SAB of Cornerstone/Rafael Pharmaceuticals. G.G. receives research funds from IBM and Pharmacyclics. W.G. receives patent royalties from FATE Therapeutics and is on the SAB of Camp4 Therapeutics.

References

1. Howlader N. et al. SEER cancer statistics review, 1975–2011. National Cancer Institute http://seer.cancer.gov/csr/1975_2011/ (2014).
2. Rustgi AK Familial pancreatic cancer: genetic advances. Genes Dev. 28, 1–7 (2014). [PubMed: 24395243]
3. Williams CL A new signaling paradigm to control the prenylation and trafficking of small GTPases. Cell Cycle 12, 2933–2934 (2013). [PubMed: 23974087]
4. Chopra SS et al. Inherited CHST11/MIR3922 deletion is associated with a novel recessive syndrome presenting with skeletal malformation and malignant lymphoproliferative disease. Mol. Genet. Genom. Med 3, 413–423 (2015).

5. Berghmans S. et al. tp53 mutant zebrafish develop malignant peripheral nerve sheath tumors. Proc. Natl Acad. Sci. USA 102, 407–412 (2005). [PubMed: 15630097]
6. Spitsbergen JM et al. Neoplasia in zebrafish (Danio rerio) treated with 7,12-dimethylbenz[a]anthracene by two exposure routes at different developmental stages. Toxicol. Pathol 28, 705–715 (2000). [PubMed: 11026607]
7. Li Q. et al. Evaluation of the novel gene Rabl3 in the regulation of proliferation and motility in human cancer cells. Oncol. Rep 24, 433–440 (2010). [PubMed: 20596630]
8. Sowa ME, Bennett EJ, Gygi SP & Harper JW Defining the human deubiquitinating enzyme interaction landscape. Cell 138, 389–403 (2009). [PubMed: 19615732]
9. Berg TJ et al. Splice variants of SmgGDS control small GTPase prenylation and membrane localization. J. Biol. Chem 285, 35255–35266 (2010). [PubMed: 20709748]
10. Schuld NJ et al. SmgGDS-558 regulates the cell cycle in pancreatic, non-small cell lung, and breast cancers. Cell Cycle 13, 941–952 (2014). [PubMed: 24552806]
11. Ntantie E. et al. An adenosine-mediated signaling pathway suppresses prenylation of the GTPase Rap1B and promotes cell scattering. Sci. Signal 6, ra39 (2013).
12. Berndt N, Hamilton AD & Sebti SM Targeting protein prenylation for cancer therapy. Nat. Rev. Cancer 11, 775–791 (2011). [PubMed: 22020205]
13. Jones S. et al. Core signaling pathways in human pancreatic cancers revealed by global genomic analyses. Science 321, 1801–1806 (2008). [PubMed: 18772397]
14. Waddell N. et al. Whole genomes redefine the mutational landscape of pancreatic cancer. Nature 518, 495–501 (2015). [PubMed: 25719666]
15. Drosten M. et al. Genetic analysis of Ras signalling pathways in cell proliferation, migration and survival. EMBO J. 29, 1091–1104 (2010). [PubMed: 20150892]
16. Rauen KA The RASopathies. Annu. Rev. Genom. Hum. Genet 14, 355–369 (2013).
17. Wang W. et al. Mice lacking Nf1 in osteochondroprogenitor cells display skeletal dysplasia similar to patients with neurofibromatosis type I. Hum. Mol. Genet 20, 3910–3924 (2011). [PubMed: 21757497]
18. Hernandez-Porras I. et al. K-RasV14I recapitulates Noonan syndrome in mice. Proc. Natl Acad. Sci. USA 111, 16395–16400 (2014). [PubMed: 25359213]
19. Roberts NJ et al. Whole genome sequencing defines the genetic heterogeneity of familial pancreatic cancer. Cancer Discov. 6, 166–175 (2016). [PubMed: 26658419]
20. Wheeler DB, Zoncu R, Root DE, Sabatini DM & Sawyers CL Identification of an oncogenic RAB. Protein Sci. 350, 211–217 (2015).
21. Jindal GA et al. In vivo severity ranking of Ras pathway mutations associated with developmental disorders. Proc. Natl Acad. Sci. USA 114, 510–515 (2017). [PubMed: 28049852]
22. Li H. & Durbin R. Fast and accurate short read alignment with Burrows– Wheeler transform. Bioinformatics 25, 1754–1760 (2009). [PubMed: 19451168]
23. DePristo MA et al. A framework for variation discovery and genotyping using next-generation DNA sequencing data. Nat. Genet 43, 491–498 (2011). [PubMed: 21478889]
24. Cox AG et al. Yap reprograms glutamine metabolism to increase nucleotide biosynthesis and enable liver growth. Nat. Cell Biol 18, 886–896 (2016). [PubMed: 27428308]
25. Love MI, Huber W. & Anders S. Moderated estimation of fold change and dispersion for RNA-seq data with DESeq2. Genome Biol. 15, 550 (2014). [PubMed: 25516281]
26. Behrends C, Sowa ME, Gygi SP & Harper JW Network organization of the human autophagy system. Nature 466, 68–76 (2010). [PubMed: 20562859]
27. Huttlin EL et al. The BioPlex network: a systematic exploration of the human interactome. Cell 162, 425–440 (2015). [PubMed: 26186194]
28. Rauniyar N. Parallel reaction monitoring: a targeted experiment performed using high resolution and high mass accuracy mass spectrometry. Int. J. Mol. Sci 16, 28566–28581 (2015). [PubMed: 26633379]
29. MacLean B. et al. Skyline: an open source document editor for creating and analyzing targeted proteomics experiments. Bioinformatics 26, 966–968 (2010). [PubMed: 20147306]

30. Krieger E. et al. Improving physical realism, stereochemistry, and side-chain accuracy in homology modeling: four approaches that performed well in CASP8. Proteins 77, 114–122 (2009). [PubMed: 19768677]

31. Xu D. & Zhang Y. Ab initio protein structure assembly using continuous structure fragments and optimized knowledge-based force field. Proteins 80, 1715–1735 (2012). [PubMed: 22411565]

32. Pierce BG, Hourai Y. & Weng Z. Accelerating protein docking in ZDOCK using an advanced 3D convolution library. PLoS ONE 6, e24657 (2011).

33. Ouyang H. et al. Response of immortalized murine cementoblasts/periodontal ligament cells to parathyroid hormone and parathyroid hormone-related protein in vitro. Arch. Oral. Biol 45, 293–303 (2000). [PubMed: 10708669]

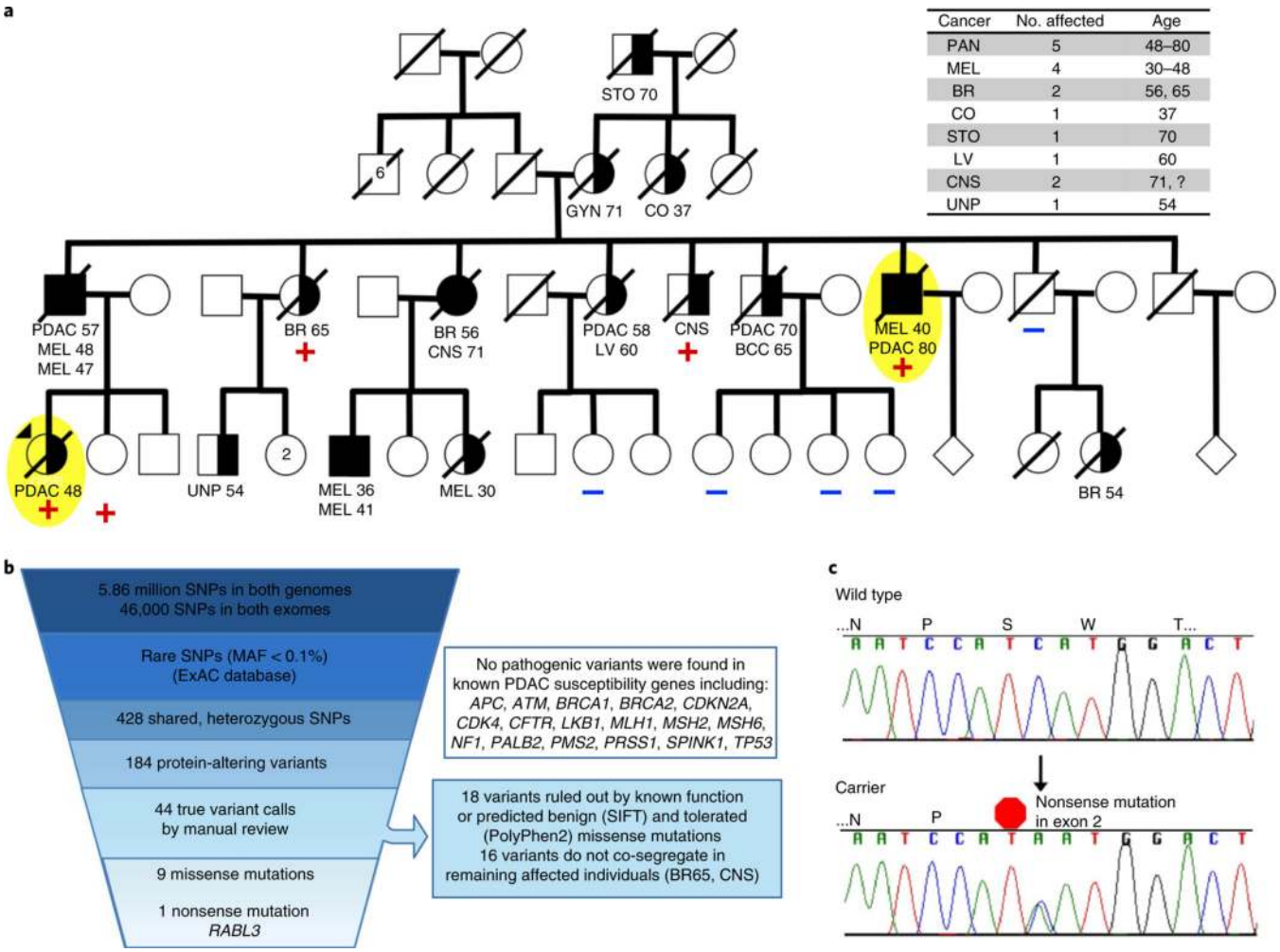

Fig. 1 |. Whole-genome sequencing in a family cluster of pancreatic cancer identifies a germline nonsense mutation in *RABL3*.

a, Pedigree of a family with high incidence of PDAC and other cancers including melanoma (MEL), breast (BR), colon (CO), stomach (STO), liver (LV), brain (CNS), unspecified gynecologic (GYN) and unknown primary (UNP) cancers. Age of tumor diagnosis is shown. Proband with index diagnosis is indicated by an arrowhead. The two individuals in whom WGS was performed are highlighted in yellow. Presence (+) or absence (–) of the *RABL3_p.Ser36** mutant germline allele as detected by Sanger sequencing is shown below each individual for whom a blood sample was available, with statistically significant co-segregation ($P = 0.0476$, Fisher's exact test). **b**, Filter-based computational algorithm used to narrow candidate variants, as detailed in the Methods. The number of variants at each step is shown. **c**, Chromatograms of *RABL3* exemplifying the wild type or the heterozygous nonsense mutation in carriers indicated in the pedigree with (+).

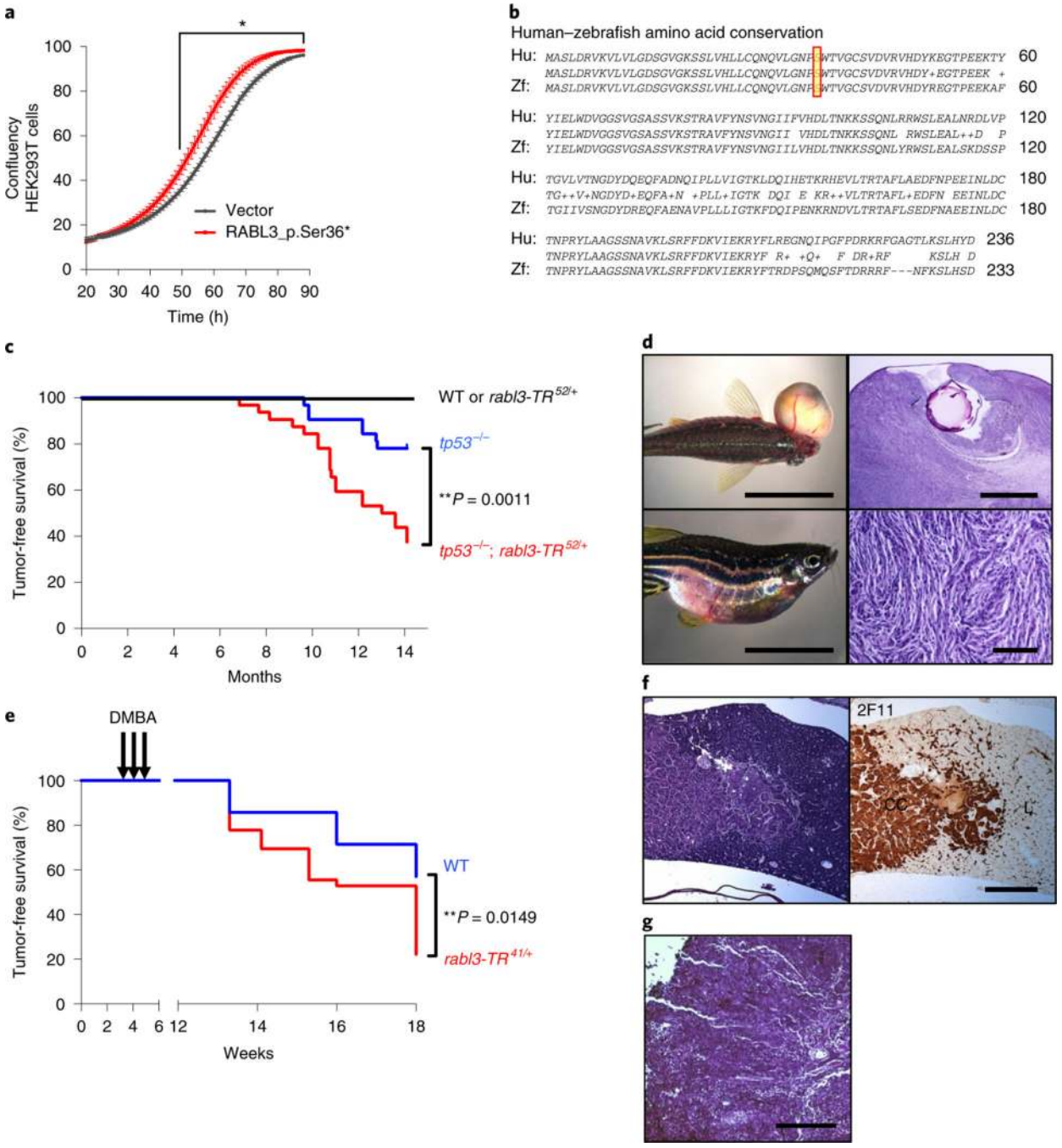

Fig. 2 |. *RABL3* mutation promotes cell proliferation in vitro and cancer in zebrafish.

a, The impact of RABL3_p.Ser36* or vector control on HEK293T cell proliferation. Graph represents mean ± s.e.m. of five independent experiments, each with ≥5 replicates. *P-< 0.05 by unpaired two-tailed t-test, with Holm–Sidak correction for multiple comparisons. **b**, Amino-acid sequence alignment of human RABL3 and zebrafish Rabl3 proteins. The Ser 36* mutation in the PDAC family is highlighted. **c**, Tumor incidence of $tp53^{-/-}$; $rabl3\text{-}TR^{52}$ heterozygous versus $tp53^{-/-}$ zebrafish. The $rabl3\text{-}TR^{52}$ allele accelerates formation of MPNSTs (N=64, P = 0.0011, log-rank Mantel–Cox test). **d**, Representative periocular or

abdominal MPNSTs; scale bars, 1cm. Histopathological analysis reveals predominantly spindle cells characteristic of MPNSTs[5]; scale bar, 1mm (top), 100μm (bottom), $N \geq 3$. **e**, Kaplan–Meier tumor-free survival curve through 18 weeks of wild-type versus *rabl3-TR*^{41} heterozygous zebrafish following DMBA exposure at weeks 3, 4 and 5. At 18 weeks, all surviving zebrafish were killed and incidence of tumors was assessed by histological survey. The *rabl3-TR*^{41} allele increases cancer formation (N=57, P=0.0149, log-rank Mantel–Cox test). WT, wild type. **f**, Histopathologic analysis of occult cholangiocarcinoma found in *rabl3-TR*^{41} heterozygous zebrafish following DMBA exposure. Biliary epithelial staining (2F11 antibody) is shown on the right, consistent with a cholangiocarcinoma. L, liver; CC, cholangiocarcinoma. Scale bar: 200μm, N=2. **g**, Representative histopathologic analysis of occult hepatocellular carcinoma found in zebrafish heterozygous for a *rabl3-TR*^{41} allele following DMBA exposure. Scale bar: 200μm, $N \geq 3$.

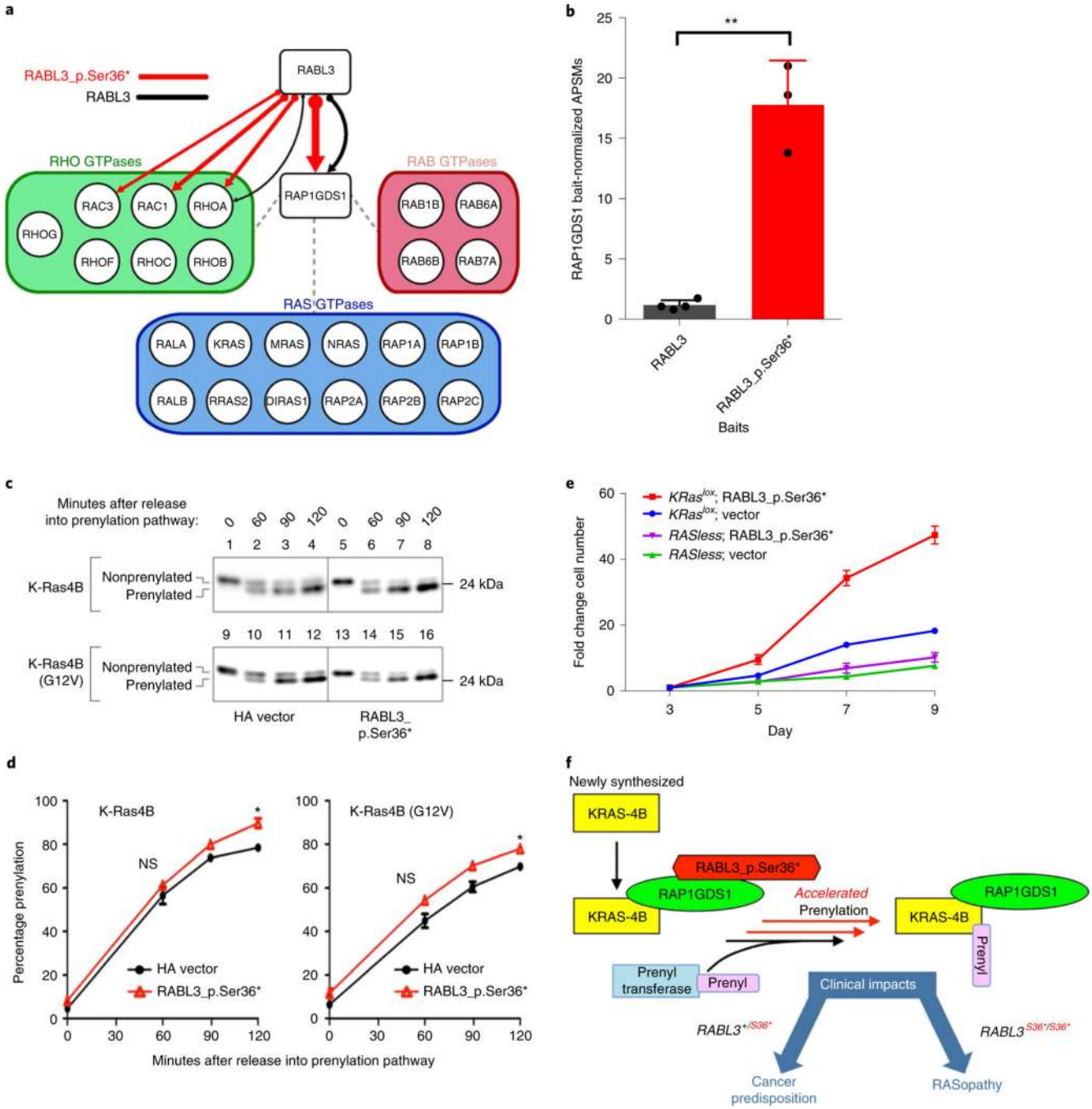

Fig. 3 |. *RABL3* mutation dysregulates KRAS activity.

a, Integrated interaction map of the RABL3 and RABL3_p.Ser36* network showing high-confidence candidate interacting proteins. Thickness of RABL3 (black) and RABL3_p.Ser36* (red) arrows denotes NWD scores. RAP1GDS1 interactors identified by AP–MS with RAP1GDS1-tagged bait are grouped by protein family for clarity and denoted by dashed gray lines. **b**, RAP1GDS1 bait-normalized APSMs for RABL3 versus RABL3_p.Ser36* AP–MS. Graph represents mean ± s.d., independent biological replicates $N = 3$ for RABL3_p.Ser36*, $N=4$ for RABL3. **$P=0.0014$ by unpaired two-tailed t-test ($t=$

7.813, d.f.=4). **c**,**d**, Impact of RABL3_p.Ser36* on KRAS-4B prenylation rate revealed by mevastatin block and-release assay. HEK293T cells were cotransfected with HA-tagged RABL3_p.Ser36* (lanes 5–8 and 13–16) or HA vector (lanes 1–4 and 9–12) and myc-tagged KRAS-4B (lanes 1–8) or myc-tagged KRAS-4B (G12V) (lanes 9–16) (**c**). Cell lysates were immunoblotted for myc at the indicated times following mevastatin block-and-release. Graphs show percentage prenylation of KRAS determined by densitometry of immunoblots (**d**). Graphs show mean ± s.e.m. from three independent experiments. NS, not significant (at 60min). At 120min, $*P = 0.014$ for KRAS-4B, $*P = 0.040$ for KRAS-4B (G12V) by unpaired two-tailed *t*-test. **e**, Impact of RABL3_p.Ser36* or vector control on proliferation of $KRas^{lox}$ or *RASless* MEFs. Graphs represent mean ± s.d. of fold change in absolute cell number in biologic triplicates per time point. **f**, Model for how RABL3_p.Ser36* may promote cancer. RABL3_p.Ser36* interacts with RAP1GDS1 and accelerates KRAS prenylation. Heterozygous patient and zebrafish carriers of RABL3_p.Ser36* exhibit cancer predisposition, whereas homozygous zebrafish carriers exhibit pleiotropic abnormalities consistent with a RASopathy syndrome. These effects of RABL3_p.Ser36* may result from chronic acceleration of KRAS prenylation.

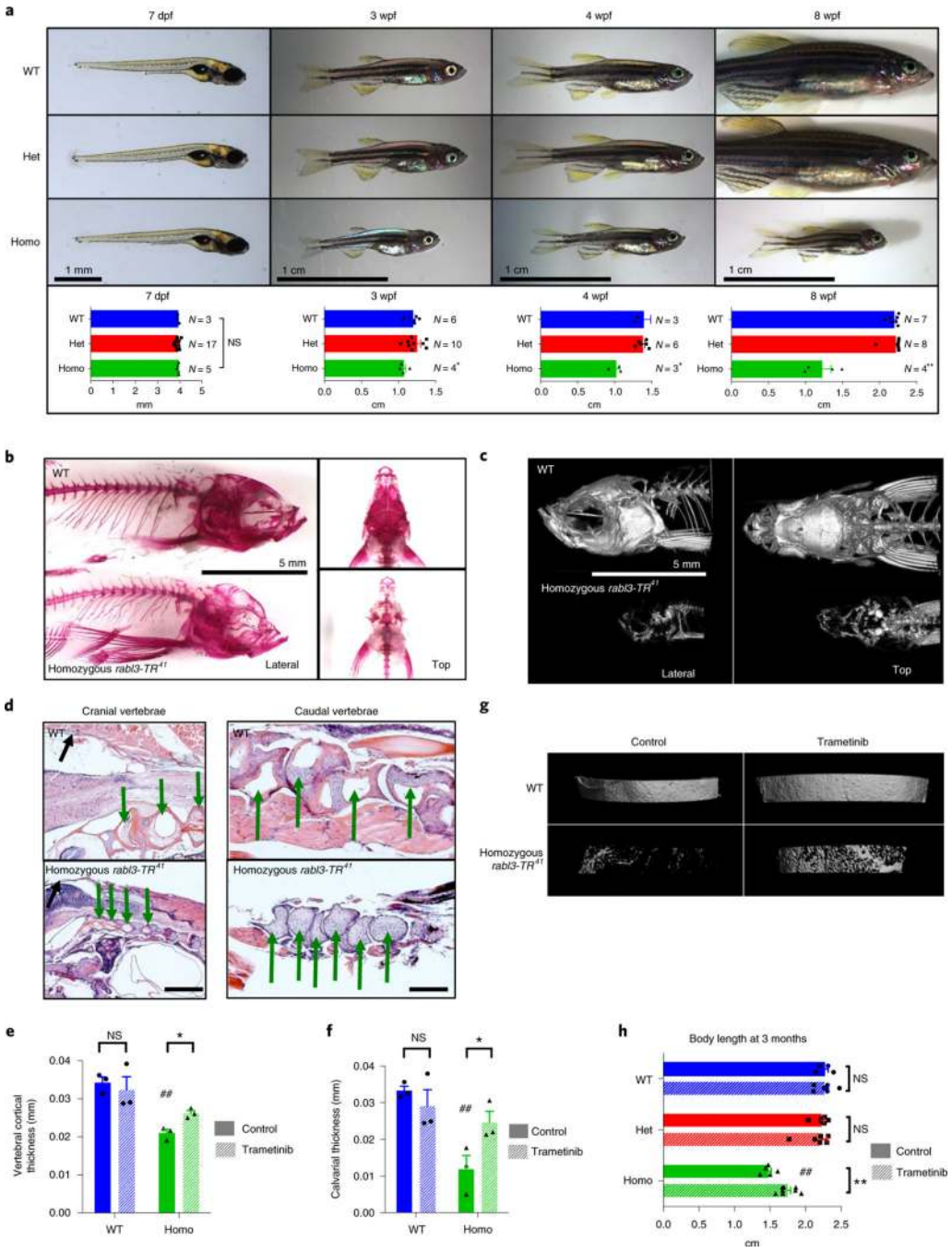

Fig. 4 |. Homozygous *rabl3-TR* mutants resemble human RASopathy syndromes.

a, Appearance and body length of wild-type and *rabl3-TR*^{41} mutant zebrafish. Mean ± s.e.m, $N \geq 3$ zebrafish. *$P = 0.0203$ (3 weeks postfertilization, wpf), *$P = 0.0463$ (4 wpf), **$P = 0.0032$ (8wpf), unpaired two-tailed *t*-test. **b**,**c**, Alizarin Red staining and 3D-μCT reveal skeletal abnormalities in homozygous *rabl3-TR*^{41} zebrafish at 3 months. Lateral and top views representative of $N \geq 3$ zebrafish of each genotype from one experiment. **d**, H&E staining of cranial and caudal vertebrae (green arrows) reveals reduced bone formation, greater cartilage content and thinner calvarium (black arrow) in *rabl3-TR*^{41} homozygous

versus wild-type zebrafish. Scale bars, 400μm. $N = 3$ zebrafish of each genotype. **e**,**f**, Histomorphometric quantification of vertebral cortical (**e**) and calvarial (**f**) thickness reveals impaired bone mineralization in *rabl3-TR*^{41} homozygous mutant versus wild-type siblings at 3 months, partially rescued when mutants were raised with trametinib. Mean ± s.e.m., $N = 3$ zebrafish of each genotype and treatment condition. Unpaired two-tailed *t*-test comparing control-treated *rabl3-TR*^{41} homozygotes to wild-type zebrafish: ##$P = 0.0016$ (**e**) and $P = 0.0053$ (**f**). Unpaired one-tailed *t*-test comparing trametinib-treated to controls: *$P = 0.0062$ (**e**) and $P = 0.0275$ (**f**). **g**, 3D-μCT of calvarium segments reveals impaired bone mineralization at 3 months in *rabl3-TR*^{41} homozygous mutant versus wild-type zebrafish, and partial rescue in mutants raised with trametinib. Top views, $N \geq 3$ zebrafish of each genotype and treatment from one experiment. **h**, Body length of wild-type and homozygous *rabl3-TR*^{41} mutants at 3 months raised with control or trametinib. Mean ± s.e.m., $N \geq 4$ zebrafish of each genotype and treatment. ##$P < 0.0001$ comparing control-treated *rabl3-TR*^{41} homozygotes to control-treated wild-type zebrafish by unpaired two-tailed *t*-test. **$P = 0.0016$ comparing trametinib-treated to control-treated *rabl3-TR*^{41} homozygotes by unpaired one-tailed *t*-test. WT, wild type; het, heterozygous; homo, homozygous.